Nonadiabatic Dynamics of Condensed Phase Rate Processes

GABRIEL HANNA* AND RAYMOND KAPRAL*

Chemical Physics Theory Group, Department of Chemistry, University of Toronto, Toronto, Ontario M5S 3H6, Canada

Received June 13, 2005

ABSTRACT

The study of quantum rate processes occurring in condensed phase environments is difficult because of the large number of degrees of freedom involved. Since a full quantum mechanical treatment is not computationally feasible, one is motivated to use mixed quantum−classical dynamical methods. This type of dynamics is applicable when one can single out a few degrees of freedom to be quantum in nature while treating the remainder classically. We describe a method that is based on the quantum−classical Liouville equation, which clearly prescribes the details of the coupling between the quantum and classical degrees of freedom. With the aid of this machinery, we show how to compute rate constants of reactions involving quantum particles immersed in a classical bath. We illustrate the use of this method on a model for proton transfer in a molecular complex dissolved in a polar solvent.

I. Introduction

While quantum mechanics provides the basis for a description of chemical rate processes, in many instances classical mechanics will capture essential elements of a chemical mechanism or predict the value of a reaction rate. There is extensive literature on classical calculations of gas and condensed phase chemical reaction rates. However, there are many situations where a classical description will not suffice. Rate processes involving the participation of multiple electronic states, relaxation of high-frequency vibrational degrees of freedom, and proton and electron transport processes are a few such examples.[1,2]

If we are interested in such quantum rate processes in the condensed phase, we are faced with a daunting task: the simulation of the quantum dynamics of a many-body system with a large number of degrees of freedom. Simulation schemes based on semiclassical methods,[3] influence−functional techniques,[4] centroid dynamics,[5] mode coupling methods,[6] and the mapping formalism[7−9] have been used to study quantum rate processes.

In many applications, only certain degrees of freedom need to be treated quantum mechanically, while the environment with which they interact can be modeled by classical mechanics to a high degree of accuracy. For example, this is the case for proton or electron transfer processes occurring in a condensed phase or other molecular environments composed of heavy atoms. This raises the issue of how to combine quantum and classical dynamics. A number of different schemes have been proposed to solve this problem. An early analysis of this problem using path integral methods was given by Pechukas.[10] The simplest scheme is adiabatic dynamics where the time-independent Schrödinger equation, $\hat{h}(R)|\alpha;R\rangle = E_\alpha(R)|\alpha;R\rangle$, for the quantum subsystem with Hamiltonian $\hat{h}(R)$ is solved for a fixed configuration of the bath molecules R to obtain the adiabatic energies $E_\alpha(R)$ and corresponding eigenvectors $|\alpha;R\rangle$. The positions and velocities of the bath molecules are then evolved using Newton's equations of motion with the Hellmann−Feynman forces, $F^\alpha(R) = -\partial E_\alpha(R)/\partial R$, determined from the adiabatic energies. Proton-transfer rates have been computed using such adiabatic methods,[11−13] where the dynamics is assumed to take place on a single protonic adiabatic energy surface.

Adiabatic methods fail when the time scales of the motions of the quantum subsystem and the bath molecules are comparable. To circumvent this problem, mean field and surface-hopping schemes have been proposed.[14] We describe such schemes, which do not restrict the evolution of the system to a single adiabatic state, as being nonadiabatic. In mean field descriptions, the total wave function is decomposed into a "fast" part corresponding to the light (quantum) particles and a "slow" part corresponding to the heavy (classical) particles. The time-dependent Schrödinger equation for the light particles is solved, and the resulting wave function is used to compute the force, which determines the evolution of the classical degrees of freedom. This approach fails when the mean potential is no longer able to provide an accurate picture of the dynamics. Extensions to such simple mean field treatments have been constructed.[15,16]

In surface-hopping schemes,[17−19] the wave function of the quantum subsystem is again propagated using the time-dependent Schrödinger equation. However, the classical degrees of freedom now evolve on single adiabatic potential energy surfaces, and hops between these surfaces occur according to probabilistic rules. The retention of quantum coherence is a limitation of such algorithms, and methods have been developed to incorporate decoherence effects.[12,20,21]

The nonadiabatic approach that we describe in this Account is based on the quantum−classical Liouville equation,[22−31] which specifies the evolution of the density matrix or an observable for a quantum mechanical system embedded in an environment that can be described

Gabriel Hanna received his B.Sc. in Chemistry from Laurentian University in 2001. He is currently working toward a Ph.D. in Chemistry at the University of Toronto. His graduate research is focused on the implementation of mixed quantum−classical techniques in the study of proton-transfer reactions.

Raymond Kapral received his Ph.D. from Princeton University in 1967. After postdoctoral work at MIT, he joined the faculty of the University of Toronto in 1969 where he is currently Professor of Chemistry. His research centers around the nonequilibrium statistical mechanics of condensed phase systems, quantum mechanical reaction rates, and the nonlinear dynamics of chemical systems displaced far from equilibrium.

* E-mail addresses: ghanna@cptg.chem.utoronto.ca; rkapral@cptg.chem.utoronto.ca.

10.1021/ar030281q CCC: $33.50
Published on Web 12/10/2005

classically. With such an evolution equation in hand, we then show how the rates of nonadiabatic chemical processes can be computed and discuss the nature of nonadiabatic quantum−classical dynamics.

II. Combining Quantum and Classical Dynamics

To describe nonadiabatic processes, we need to simultaneously evolve the quantum degrees of freedom along with the classical environmental degrees of freedom to which they are coupled. Although the environment may behave classically in the absence of coupling to the quantum system, this is no longer the case when they are coupled. This leads to the issue of how and whether quantum and classical descriptions can be combined. In quantum mechanics, an observable is mathematically represented by an operator $\hat{N}$ and its time evolution is governed by the Heisenberg equation, $(\mathrm{d}/\mathrm{d}t)\hat{N}(t) = i/\hbar[\hat{H},\hat{N}(t)]$, where $\hat{H}$ is the Hamiltonian and [X,Y] is the commutator. Analogously, in classical mechanics, an observable is a function $N(R,P)$ of the positions R and momenta P of all the particles in the system, and its time evolution is governed by the classical analogue of the Heisenberg equation, $(\mathrm{d}/\mathrm{d}t)N(t) = \{N(t),H\}$, where H is the classical Hamiltonian and {X,Y} is the Poisson bracket. Thus, a hybrid quantum−classical mechanics should involve an equation of motion for the observable $\hat{N}(R,P,t)$, which has both an operator character and a phase space dependence. Our approach to combining these two theories is to start with a full quantum mechanical description of the system plus its environment in terms of the quantum mechanical Liouville equation for the density matrix or, equivalently, the Heisenberg equation for a general observable, $\hat{N}$. Then, by singling out the environmental degrees of freedom for special treatment, a transformation[32] from quantum operators to phase space functions is carried out. Finally the equation is expanded in the small parameter $\mu = (m/M)^{1/2}$, where m and M are the characteristic masses of the system and environment particles, respectively. Retaining up to first order in μ, we obtain the quantum−classical Heisenberg equation,[22,23]

$$\frac{\mathrm{d}}{\mathrm{d}t}\hat{N}(R,P,t) = \frac{i}{\hbar}[\hat{H},\hat{N}(t)] - \frac{1}{2}(\{\hat{H},\hat{N}(t)\} - \{\hat{N}(t),\hat{H}\}) \quad (1)$$

which is valid in the limit $m \ll M$. This equation of motion, or the corresponding quantum−classical Liouville equation, has a structure that combines features of the quantum and classical Liouville equations. As expected, the observable is neither just $\hat{N}$ nor $N(R,P)$ but is $\hat{N}(R,P)$. The first term on the right-hand side involving the commutator [X,Y] of the Hamiltonian, $\hat{H}$, with the observable has the same structure as the quantum Heisenberg equation, while the second term involving the Poisson bracket {X,Y} of the Hamiltonian with the observable has a structure like that of the classical equations of motion for a dynamical variable. Thus, the time evolution of both the quantum and classical degrees of freedom are specified by this equation.

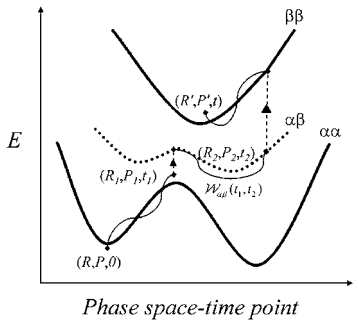

FIGURE 1. A trajectory segment with two nonadiabatic transitions starting from $(R,P,t=0)$. In the time segment between t_1 and t_2, the system evolves coherently on the mean adiabatic surface (dotted line) and the observable is multiplied by the phase factor $\mathscr{W}_{\alpha\beta}(t_1,t_2)$. The two solid lines denote the potential energy surfaces corresponding to adiabatic states α and β, respectively.

Insight into the nature of quantum−classical dynamics can be obtained by considering a matrix representation of this equation in the adiabatic basis. In this way, connection to surface-hopping dynamics can be made. In the adiabatic basis we have

$$\frac{\mathrm{d}}{\mathrm{d}t}N^{\alpha\alpha'}(R,P,t) = (i\omega_{\alpha\alpha'}(R) + iL_{\alpha\alpha'})N^{\alpha\alpha'}(t) - \sum_{\beta\beta'} J_{\alpha\alpha',\beta\beta'}N^{\beta\beta'}(t) \quad (2)$$

where $\langle\alpha;R|\hat{N}(R,P)|\alpha';R\rangle = N^{\alpha\alpha'}(R,P)$. From the right-hand side of this equation, we observe that the time evolution of $N^{\alpha\alpha'}(R,P,t)$ depends on three contributions: the frequency $\omega_{\alpha\alpha'}(R) = (E_\alpha(R) - E_{\alpha'}(R))/\hbar$, which involves the difference of adiabatic energies, $iL_{\alpha\alpha'}$, which determines the classical evolution of the bath degrees of freedom governed by the mean of the Hellmann−Feynman forces for states α and α', $F^{\alpha\alpha'} = -{}^1/_2\,\partial(E_\alpha + E_{\alpha'})/\partial R$, and $J_{\alpha\alpha',\beta\beta'}$, which accounts for the nonadiabatic quantum transitions and associated momentum changes in the bath.[22,23]

The solution of this equation can be represented in terms of an ensemble of surface-hopping trajectories. An example of such a trajectory is shown schematically in Figure 1. This trajectory starts on the ground adiabatic potential energy surface at bath coordinates (R,P) and the observable is described by $N^{\alpha\alpha}(R,P,0)$. Two nonadiabatic transitions occur in the subsequent evolution. The first nonadiabatic transition takes place at time t_1 and involves the quantum transition $\alpha\alpha \rightarrow \alpha\beta$. This transition puts the system in the coherent quantum state, and the observable can now be described by the off-diagonal matrix element $N^{\alpha\beta}(R_1,P_1,t_1)$. Moreover, it is accompanied by a change in the momenta of the bath particles such that the corresponding kinetic energy change compensates for the fact that the energy of the coherent state is the mean of the energies of adiabatic states α and β, $(E_\alpha(R) + E_\beta(R))/2$, thereby conserving the total energy of the system. Between t_1 and t_2, the classical degrees of freedom evolve by Newton's equations of motion governed by the mean of the Hellmann−Feynman forces for quantum states α and β. The quantum system evolves coherently, and a phase

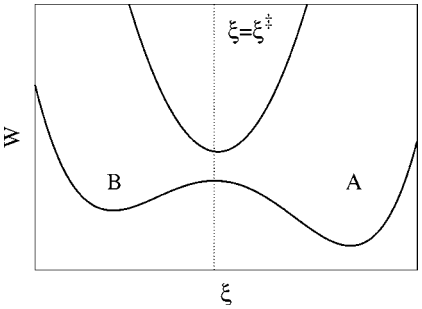

FIGURE 2. Ground adiabatic state free energy surface with a double-well structure and the first excited adiabatic free energy surface with a single minimum.

$\mathscr{W}'_{\alpha\beta}(t_1,t_2) = \exp(i\int_{t_1}^{t_2} dt'\ \omega_{\alpha\beta}(R(t')))$ accumulates in the observable along this segment of the trajectory. At time t_2, a second nonadiabatic transition $\alpha\beta \rightarrow \beta\beta$ takes place, giving rise to the diagonal matrix element $N^{\beta\beta}(R_2,P_2,t_2)$. The quantum coherence is destroyed as a result of this transition. The subsequent evolution to time t takes place on the single adiabatic potential energy surface $E_\beta(R)$ giving $N^{\beta\beta}(R',P',t)$ at bath coordinates (R',P'). Finally, the matrix element $N^{\alpha\alpha'}(R,P,t)$ is appropriately constructed[33,34] from all such trajectories in which quantum transitions can occur stochastically at any intermediate time.

There is a major difference between the surface-hopping dynamics that generates the solution of the quantum−classical Liouville equation and other surface-hopping schemes.[12,17] Typically, in such schemes, the time-dependent Schrödinger equation for the quantum system is evolved in conjunction with an assumed form of the evolution of the classical bath coordinates. In particular, the classical degrees of freedom evolve according to Newton's equations of motion on single adiabatic energy surfaces between the quantum transitions. Thus, the coherent evolution segments discussed above do not appear in the description. The quantum−classical Liouville or Heisenberg equations specify the evolution of both the quantum and classical degrees of freedom so that no additional ansatz about the nature of the classical dynamics is required. We now turn to a discussion of the implications of such nonadiabatic dynamics for the calculation of chemical reaction rates.

III. Nonadiabatic Reaction Rates

Suppose that the reactive dynamics of a system can be described in terms of a reaction coordinate $\xi(R)$, which is assumed to be some function of the bath coordinates alone. At this point, the description is still general and we do not specify the physical nature of the adiabatic states, which could be electronic, protonic, or vibrational, for example. The situation that we wish to study is the case where the free energy, $W(\xi)$, along this reaction coordinate has an asymmetric double-well form when the system is in the ground adiabatic state and a single minimum when the system is in the first excited adiabatic state. The free energy profiles are shown in Figure 2. A dividing surface at $\xi(R) = \xi^\ddagger$ serves to partition the reaction coordinate of the system into two domains, which contain the metastable A and B species, respectively. The microscopic variable corresponding to the density of species A is $N_A(R) = \theta(\xi(R) - \xi^\ddagger)$, where θ is the Heaviside function. Similarly, the microscopic variable corresponding to the density of species B is $N_B(R) = \theta(\xi^\ddagger - \xi(R))$. The metastable states A and B corresponding to the system localized to the right and left of the free energy barrier interconvert, A ⇌ B, and we wish to determine the rate constant for this process.

If we assume that the system obeys adiabatic dynamics and its evolution takes place on the ground state adiabatic surface $E_1(R)$ only, the problem is simple. The bath degrees of freedom evolve by Newton's classical equations of motion, and the quantum nature of the problem only enters through the ground state Hellmann−Feynman forces, $F^1(R) = -\partial E_1(R)/\partial R$. Statistical mechanics tells us that the adiabatic rate constant can be determined from a reactive flux correlation function.[11,35] For the forward reaction, A → B, this correlation function can be calculated by launching trajectories from the barrier top with a given initial flux of $N_A(R)$ (determined from an equilibrium configuration of the system) and then monitoring in time whether the system is in the product or reactant state. Formally, this amounts to computing a time-dependent rate coefficient, which is expressed in terms of an equilibrium correlation function of the initial flux $\dot{N}_A(R)$ of $N_A(R)$ with $N_B(R)$ at time t as

$$k_{AB}^{ad}(t) = \frac{1}{n_A^{eq}}\int dR\, dP\, \dot{\xi}\delta(\xi(R) - \xi^\ddagger)N_B(R(t))\rho_{We}^1(R,P) \tag{3}$$

where δ is the Dirac delta function, n_A^{eq} is the equilibrium density of species A, and we have used $\dot{N}_A(R) = \dot{\xi}(R)\delta(\xi(R) - \xi^\ddagger)$. The weight of each point (R,P) in the phase space integral is given by the canonical equilibrium density matrix element for the system in the adiabatic ground state, $\rho_{We}^1(R,P) = Z^{-1}\exp(-\beta H_W^1)$, where $Z = \int dR\, dP \exp(-\beta H_W^1)$ is the partition function with the ground state Hamiltonian $H_W^1 = P^2/(2M) + E_1(R)$. The time-dependent rate coefficient $k_{AB}^{ad}(t)$ will decay from its initial transition state theory value, $k_{AB}^{ad}(t = 0+) = k_{AB}^{ad,TST}$,[36] to a plateau value if there is a substantial time scale separation between the microscopic and chemical relaxation times.[37] The plateau value determines the measured rate constant, k_{AB}^{ad}, for the reaction.

The nonadiabatic rate formula differs from that for adiabatic dynamics as a result of two new features.[38] First, the time evolution of the species variable follows quantum−classical nonadiabatic dynamics so that transitions to excited states occur. Second, the equilibrium density matrix has a form in which off-diagonal elements appear due to the retention of quantum coherence in the initial weights. Instead of the simple form for ρ_{We}^1 given above, we now have $\rho_{We}^{\alpha\alpha'}$ for which the diagonal contribution is $\rho_{We}^{\alpha} = Z_0^{-1}\exp(-\beta H_W^\alpha)$ with $Z_0 = \sum_\alpha \int dR\, dP \exp(-\beta H_W^\alpha)$, as well as the off-diagonal contributions.[39] In the application, we consider that the diagonal parts of the density

matrix give the major contribution to the rate, and we have

$$k_{AB}(t) \simeq -\frac{1}{n_A^{eq}}\sum_{\alpha=1}^{2}\int dR\, dP\, \dot{\xi}(R) N_B^{\alpha\alpha}(R,P,t)\delta(\xi(R)-\xi^{\ddagger})\rho_{We}^{\alpha}(R,P) \quad (4)$$

As for adiabatic dynamics, trajectories are started at the barrier top and the rate constant is obtained from the plateau value of $k_{AB}(t)$.

IV. Proton Transfer

To illustrate these ideas, we consider a two-state model for a proton-transfer reaction (AH−B ⇌ A^-−H^+B) in a hydrogen-bonded complex (AHB) that is dissolved in a polar solvent.[33] The potential energy function describing the hydrogen bonding within the complex is chosen to model a slightly strong hydrogen bond between the hydroxyl and amine groups in phenol (A) trimethylamine (B) in the absence of a solvent.[40] We assume that the dynamics of the proton is electronically adiabatic. Over the years, this model has been subject to intensive study.[12,40−45] In our investigation, the AB distance is fixed to be 2.7 Å. At this separation, the potential energy function has two minima, which correspond to the stable covalent and metastable ionic states of the complex. The charge distribution in the complex can shift as the proton moves along the AB bond. The solvent potential energy functions model nonpolarizable methyl chloride molecules.

The Hamiltonian operator, partially transformed[32] over the coordinates of the solvent and A and B groups of the complex, is given by

$$\hat{H}(\hat{q},R) = K_S + K_C + \hat{H}_P(\hat{q},R) \quad (5)$$

where $\hat{H}_P(\hat{q},R) = \hat{K}_P + \hat{V}(\hat{q},R)$ is the protonic Hamiltonian for a fixed set of classical coordinates. The protonic kinetic energy operator is $\hat{K}_P$, while K_S and K_C denote the classical kinetic energy contributions from the solvent and complex, respectively. The solvent and A and B groups of the complex, whose positions are denoted by R, are the classical particles. The proton, whose position is described by the operator $\hat{q}$, comprises the quantum subsystem. In this study, the adiabatic surfaces correspond to the eigenstates of the protonic Hamiltonian; the electronic degrees of freedom are accounted for in the model potential functions.

The proton-transfer reaction can be monitored by observing the evolution of the mean position of the proton in the ground adiabatic state ($\langle q\rangle(R)$), and by the solvent polarization ($\Delta E(R)$),[46,47] which is the difference between the solvent electrical potentials at two points within the complex corresponding to the minima of the bare hydrogen bonding potential. Both of these reaction coordinates are functions of all of the positions of the classical particles.

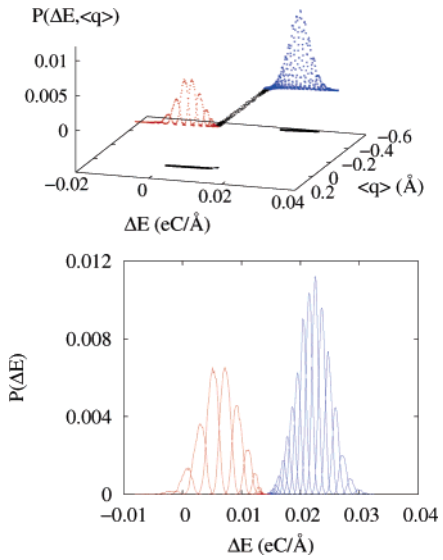

FIGURE 3. Joint probability histogram, $P(\Delta E,\langle q\rangle)$ (top), of the mean position of the proton ($\langle q\rangle$) in the ground state and the solvent polarization (ΔE) and projection of the above histogram (bottom) onto a $P-\Delta E$ plane. The various curves correspond to different $\langle q\rangle$ values.

The essentials of the proton-transfer mechanism can be inferred from the histogram at the top of Figure 3. It was generated by simultaneously binning the time series of $\langle q\rangle$ and ΔE from a long trajectory on the ground state adiabatic surface. Starting in the covalent state ($\langle q\rangle \approx 0$ Å, $\Delta E \approx 0.005$ eC/Å), we see that the solvent undergoes an extensive polarization to induce a large shift in the protonic charge, followed by a relaxation of the solvent in response to the new ionic state ($\langle q\rangle \approx -0.57$ Å, $\Delta E \approx 0.0225$ eC/Å). The transfer of the proton only occurs for a narrow window of ΔE values. The time scale of this process can be estimated by examining some sample proton hops; the entire process takes place in several hundreds of femtoseconds, but the actual transfer of the proton occurs rapidly in only a few tens of femtoseconds. The histogram also tells us that the complex spends more time in the ionic configuration than in the covalent configuration. This is because electrostatic interactions with the polar solvent preferentially stabilize the ionic configuration, in contrast to the gas phase where the covalent configuration is more stable. If we project this histogram onto a $P-\Delta E$ plane (see bottom of Figure 3), sum over all the $\langle q\rangle$ contributions at each value of ΔE, and take the negative logarithm of this new probability, we obtain a free energy profile along the ΔE reaction coordinate that has the same asymmetric double-well structure as the ground adiabatic free energy profile in Figure 2. The first excited state free energy surface for this system has a single-well structure like that in Figure 2; hence, these features correspond to the situation that we set out to study. There is a large free energy difference between the first and second excited state surfaces, so the second excited state is not expected to participate strongly in the nonadiabatic dynamics.

The adiabatic rate coefficient, $k_r^{ad}(t)$, for the reverse proton-transfer reaction was determined from a calcula-

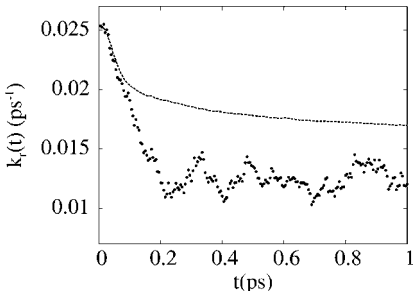

FIGURE 4. Comparison between the nonadiabatic (points) and adiabatic (line) reverse rate coefficients as a function of time.

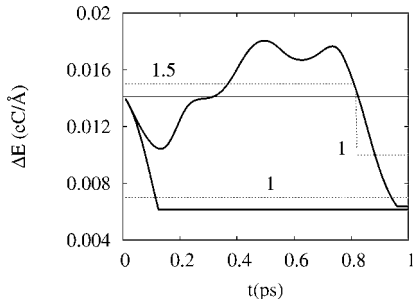

FIGURE 5. $\Delta E(t)$ (thick solid lines) and quantum state (dotted lines) along two sample nonadiabatic trajectories that start at the barrier top. The thin solid line denotes the position of the barrier top. When the system commits itself to one of its stable configurations, the trajectory is terminated and $\Delta E(t)$ remains constant for the remainder of the time.

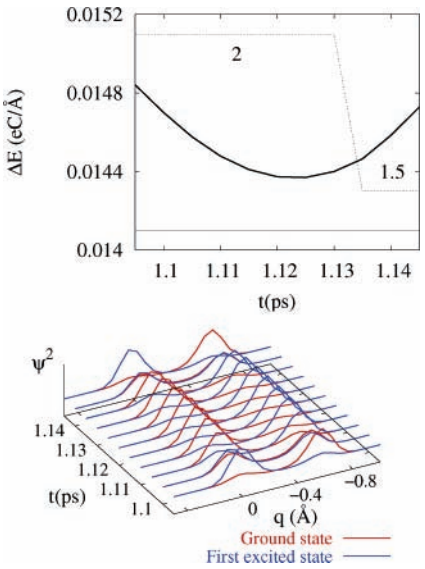

FIGURE 6. $\Delta E(t)$ (thick solid line) and quantum state (dotted line) along a segment of a nonadiabatic trajectory (top), the thin solid line denoting the position of the barrier top, and probability densities (bottom) corresponding to the ground and first excited state adiabatic wave functions (ψ^2) as a function of the protonic coordinate (q) along this segment.

tion of eq 3 employing $\xi(R) = \Delta E(R)$ as the reaction coordinate and $\xi^{\ddagger} = \Delta E^{\ddagger} = 0.0141$ eC/Å as the dividing surface. The ensemble average needed to compute $k_r^{ad}(t)$ is conditioned on the reaction coordinate being at this dividing surface. For highly activated rate processes, this would pose a problem since the system would rarely visit the barrier top. To circumvent this problem, the conditional average can be efficiently computed using "blue moon" sampling,[48] which fixes the reaction coordinate at $\Delta E = \Delta E^{\ddagger}$ at $t = 0$ for every trajectory in the ensemble. Each trajectory is then initialized by releasing the constraint and appropriately resampling the particle velocities. In the nonadiabatic case, where coupling between the solvent motions and the quantum protonic degree of freedom can induce quantum transitions among the adiabatic states, the rate coefficient $k_r(t)$ was calculated from eq 4 using the same sampling scheme as that for the adiabatic rate calculation.

In Figure 4, we present results for the time-dependent adiabatic and nonadiabatic rate coefficients, which were obtained from an average over 16 000 trajectories. As expected, we see that the rate coefficients fall quickly from their initial transition state theory values in a few tenths of a picosecond to plateaus from which the rate constants can be extracted. The decrease in the rate coefficient from its transition state theory value is due to recrossing by the trajectory of the barrier top before the system reaches a stable state. The values of k_r^{ad} and k_r obtained from the plateaus are $k_r^{ad} = 0.017$ ps^{-1} and $k_r = 0.013$ ps^{-1}.

To understand why the nonadiabatic rate constant is lower than the adiabatic rate constant, we must examine the trajectories involved in the simulation of the nonadiabatic rate coefficient. Figure 5 depicts two such trajectories. The lower trajectory, like in adiabatic dynamics, does not make any quantum transitions throughout the course of its evolution, remaining on the ground state surface (denoted by 1). It quickly settles into the covalent well. In contrast, the upper trajectory immediately hops onto the coherent state surface (denoted by 1.5) and remains there for 0.8 ps until it falls back down to the ground state surface. These nonadiabatic transitions occur when the trajectory is in the vicinity of the barrier top (since the probability of a transition is highest in this region according to our sampling scheme[33,34]). We note that the dynamics on the coherent state surface is associated with excursions in $\Delta E(t)$ across the barrier top. These recrossings delay the occurrence of a reactive event. As a result of this frustrated proton transfer, the reactive flux correlation function will decay more quickly and thereby reduce the rate constant. Since a substantial number of trajectories in the ensemble visit the coherent state surface and, as seen in Figure 5, the system can spend a considerable amount of time on the coherent state surface, the role of the coherent state surface is crucial for this rate process.

Figure 6 shows the solvent polarization and quantum state along a short segment of another trajectory. In this segment, the system evolves initially on the first excited adiabatic state surface (denoted by 2) and then on the mean of the ground and first excited state adiabatic surfaces. The system tends to linger in the neighborhood of the barrier top due to the forms of these surfaces. When on the excited surface, the system is expected to be confined to the barrier top region. On the mean surface, the system will also visit the barrier region frequently since the mean of the ground and excited state surfaces has a

low barrier. While the evolution of the matrix elements of the species variable, $N_B^{\alpha\alpha'}(R,P,t)$, is determined by the quantum−classical Liouville equation as described above, an examination of the time evolution of the adiabatic wave functions along the quantum−classical trajectory is interesting, since it reflects the changes in the solvation structure of the proton complex in the vicinity of the barrier top. At two points along this trajectory, the character of the ground state wave function switches from ionic to covalent and from covalent to ionic and vice versa for the first excited state wave function. These character swaps occur in approximately 5−10 fs. Thus, we see that when ΔE is near the barrier top, certain solvent fluctuations may cause rapid and drastic switches in the characters of the adiabatic wave functions. This behavior is consistent with the information presented in the top portion of Figure 3, where we saw a wide spread of $\langle q \rangle$ values for a narrow window of ΔE values around the barrier top. When the system eventually drops to the ground state, the solvent molecules are then able to reorganize in such a way to stabilize the covalent form of the complex (AH−B). During this process, the characters of the adiabatic wave functions do not change and the ground state probability density (localized in the covalent state) increases, while the excited state probability density (localized in the ionic state) decreases. Nonadiabatic dynamics enhances these effects since a large fraction of trajectories in the ensemble linger in the barrier region.

V. Concluding Remarks

The rates and mechanisms of quantum rate processes occurring in condensed phase environments are difficult to determine because simulating quantum dynamics in many-body environments is a formidable task. This problem may be circumvented by taking a mixed quantum−classical approach since the environment is typically composed of molecules that are much heavier than the quantum particle being transferred in the reaction. When coupling between the quantum and classical degrees of freedom induces transitions among the adiabatic states, the adiabatic approximation breaks down and nonadiabatic dynamics must be implemented. We have shown that quantum−classical Liouville dynamics in conjunction with the quantum−classical reactive flux expression for the nonadiabatic rate can be used to study condensed phase quantum rate processes.

Although the solution of the quantum−classical Liouville equation can be represented in terms of an ensemble of surface-hopping trajectories, the nature of these trajectories is quite different from that in standard surface-hopping schemes. In the quantum−classical Liouville approach, trajectories are generated by classical evolution, either on single adiabatic surfaces or on the mean of two adiabatic surfaces of a coherently coupled pair of states. Furthermore, during the coherent evolution segments, the observable of interest accumulates a phase to reflect the creation of quantum coherence. In addition to creating and destroying quantum coherence throughout the evolution, the quantum−classical propagator ensures that energy is exactly conserved along a trajectory even if the momentum-jump approximation[33] is made. Of course, physical significance should only be attached to expectation values computed from averages over the ensemble.

For highly activated rate processes, one cannot simply track the dynamics over many reactive events because chemical reactions take place on time scales that are long compared to typical microscopic relaxation times accessible in computer simulations. Consequently, one must implement rare event sampling schemes to compute the reaction rate. We used one such method, "blue moon" sampling, which enabled us to obtain the rate constant from short-time simulations of the dynamics. Conveniently, because of the use of the solvent polarization as the reaction coordinate, the quantum−classical reactive flux formulas for the rate have a simple form that allows one to easily implement this sampling scheme.

An aspect of our results on intermolecular proton transport is worth emphasizing. In the dynamics of the trajectories contributing to the ensemble used to compute the nonadiabatic rate constant, the mean surface plays a crucial role. When a quantum transition takes the system from the ground state to the coherent state, the solvent polarization tends to fluctuate around its transition state value. The next quantum transition, which takes the system either back to the ground state or to the first excited state, destroys the coherence created in the first transition. This enhanced barrier recrossing lowers the reaction rate. This picture of how quantum transitions reduce the reaction rate is quite different from that in standard surface-hopping methods.

The techniques outlined in this Account for performing quantum−classical dynamics and computing reaction rates may be applied to a large class of systems for which a proper description requires quantum mechanical intervention. As the level of complexity of such systems rises, one may supplement these methods with other relevant computational tools. Since full-scale quantum mechanical calculations of large systems are intractable, further development of algorithms used to execute quantum−classical dynamics is a worthwhile effort.

This work was supported in part by a grant from the Natural Sciences and Engineering Research Council of Canada.

References

(1) Bell, R. P. *The Proton in Chemistry*; Chapmann & Hall: London, 1973.
(2) *Electron and Ion Transfer in Condensed Media*; Kornyshev, A. A., Tosi, M., Ulstrup, J., Eds.; World Scientific: Singapore, 1997.
(3) Wang, H.; Thoss, M.; Miller, W. H. Forward−backward initial value representation for the calculation of thermal rate constants for reactions in complex molecular systems. *J. Chem. Phys.* **2000**, *112*, 47−55.
(4) Topaler, M.; Makri, N. Quantum rates for a double well coupled to a dissipative bath: Accurate path integral results and comparison with approximate theories. *J. Chem. Phys.* **1994**, *101*, 7500−7519.
(5) Geva, E.; Shi, Q.; Voth, G. A. Quantum-mechanical reaction rate constants from centroid molecular dynamics simulations. *J. Chem. Phys.* **2001**, *115*, 9209−9222.

(6) Golosov, A. A.; Reichman, D. R.; Rabani, E. Analytic continuation for quantum nonadiabatic rate constants. *J. Chem. Phys.* **2003**, *118*, 457−460.
(7) Miller, W. H.; McCurdy, C. W. Classical trajectory model for electronically nonadiabatic collision phenomena. A classical analogue for electronic degrees of freedom. *J. Chem. Phys.* **1978**, *69*, 5163−5173.
(8) Stock, G.; Thoss, M. Semiclassical Description of Nonadiabatic Quantum Dynamics. *Phys. Rev. Lett.* **1997**, *78*, 578−581.
(9) Bonella, S.; Coker, D. F. LAND-map, a linearized approach to nonadiabatic dynamics using the mapping formalism. *J. Chem. Phys.* **2005**, *122*, No. 194102 (13 pages).
(10) Pechukas, P. Time-dependent semiclassical scattering theory. II. Atomic Collisions. *Phys. Rev.* **1969**, *181*, 174−185.
(11) Laria, D.; Ciccotti, G.; Ferrario, M.; Kapral, R. Molecular-dynamics study of adiabatic proton-transfer reactions in solution. *J. Chem. Phys.* **1992**, *97*, 378−388.
(12) Hammes-Schiffer, S.; Tully, J. C. Proton transfer in solution: Molecular dynamics with quantum transitions. *J. Chem. Phys.* **1994**, *101*, 4657−4667.
(13) Consta, S.; Kapral, R. Dynamics of proton transfer in mesoscopic clusters. *J. Chem. Phys.* **1995**, *104*, 4581−4590.
(14) Tully, J. C. Mixed quantum−classical dynamics: mean-field and surface-hopping. In *Classical and Quantum Dynamics in Condensed Phase Simulations*; Berne, B. J., Ciccotti, G., Coker, D. F., Eds.; World Scientific: Singapore, 1998; Chapter 21.
(15) Prezhdo, O. V. Mean field approximation for the stochastic Schrödinger equation. *J. Chem. Phys.* **1999**, *111*, 8366−8377.
(16) Brooksby, C.; Prezhdo, O. V. Quantized mean-field approximation. *Chem. Phys. Lett.* **2001**, *346*, 463−469.
(17) Tully, J. C. Molecular dynamics with electronic transitions. *J. Chem. Phys.* **1990**, *93*, 1061−1071.
(18) Webster, F.; Wang, E. T.; Rossky, P. J.; Friesner, R. A. Stationary phase surface hopping for nonadiabatic dynamics: Two-state systems. *J. Chem. Phys.* **1994**, *100*, 4835−4847.
(19) Coker, D. F.; Xiao, L. Methods for molecular dynamics with nonadiabatic transitions. *J. Chem. Phys.* **1995**, *102*, 496−510.
(20) Bittner, E. R.; Rossky, P. J. Quantum decoherence in mixed quantum−classical systems: Nonadiabatic processes. *J. Chem. Phys.* **1995**, *103*, 8130−8143.
(21) Bittner, E. R.; Schwartz, B. J.; Rossky, P. J. Quantum decoherence: a consistent histories treatment of condensed phase nonadiabatic quantum molecular dynamics. *J. Mol. Struct. (THEOCHEM)* **1997**, *389*, 203−216.
(22) Kapral, R.; Ciccotti, G. Mixed quantum−classical dynamics. *J. Chem. Phys.* **1999**, *110*, 8919−8929.
(23) Kapral, R.; Ciccotti, G. A Statistical Mechanical Theory of Quantum Dynamics in Classical Environments. In *Lecture Notes in Physics*; Nielaba, P., Mareschal, M., Ciccotti, G., Eds.; Springer-Verlag: Berlin, 2002; Chapter 16.
(24) Aleksandrov, I. V. The statistical dynamics of a system consisting of a classical and a quantum subsystem. *Z. Naturforsch.* **1981**, *36a*, 902−908.
(25) Gerasimenko, V. I. Dynamical equations of quantum−classical systems. *Theor. Math. Phys.* **1982**, *50*, 77−87.
(26) Boucher, W.; Traschen, J. Semiclassical physics and quantum fluctuations. *Phys. Rev. D* **1988**, *37*, 3522−3532.
(27) Zhang, W. Y.; Balescu, R. Statistical mechanics of a spin-polarized plasma. *J. Plasma Phys.* **1988**, *40*, 199−213.
(28) Martens, C. C.; Fang, J.-Y. Semiclassical-limit molecular dynamics on multiple electronic surfaces. *J. Chem. Phys.* **1996**, *106*, 4918−4930.
(29) Horenko, I.; Salzmann, C.; Schmidt, B.; Schütte, C. Quantum-classical Liouville approach to molecular dynamics: Surface hopping Gaussian phase-space packets. *J. Chem. Phys.* **2002**, *117*, 11075−11088.
(30) Shi, Q.; Geva, E. A derivation of the mixed quantum−classical Liouville equation from the influence functional formalism. *J. Chem. Phys.* **2004**, *121*, 3393−3404.
(31) Prezhdo, O. V.; Kisil, V. V. Mixing quantum and classical mechanics. *Phys. Rev. A* **1997**, *56*, 162−175.
(32) Wigner, E. On the quantum correction for thermodynamic equilibrium. *Phys. Rev.* **1932**, *40*, 749−759.
(33) Hanna, G.; Kapral, R. Quantum-classical Liouville dynamics of nonadiabatic proton transfer. *J. Chem. Phys.* **2005**, *122*, 244505-1−244505-11.
(34) McKernan, D.; Kapral, R.; Ciccotti, G. Sequential short-time propagation of quantum−classical dynamics. *J. Phys.: Condens. Matter* **2002**, *14*, 9069−9076.
(35) Yamamoto, T. Quantum Statistical Mechanical Theory of the Rate of Exchange Chemical Reactions in the Gas Phase. *J. Chem. Phys.* **1969**, *33*, 281−289.
(36) Chandler, D. Statistical mechanics of isomerization dynamics in liquids and the transition state approximation. *J. Chem. Phys.* **1978**, *68*, 2959−2970.
(37) Kapral, R.; Consta, S.; McWhirter, L. Chemical rate laws and rate constants. In *Classical and Quantum Dynamics in Condensed Phase Simulations*; Berne, B. J., Ciccotti, G., Coker, D. F., Eds.; World Scientific: Singapore, 1998; Chapter 24.
(38) Sergi, A.; Kapral, R. Quantum-classical dynamics of nonadiabatic chemical reactions. *J. Chem. Phys.* **2003**, *118*, 8566−8575.
(39) Nielsen, S.; Kapral, R.; Ciccotti, G. Statistical mechanics of quantum−classical systems. *J. Chem. Phys.* **2001**, *115*, 5805−5815.
(40) Azzouz, H.; Borgis, D. A quantum molecular-dynamics study of proton-transfer reactions along asymmetrical H bonds in solution. *J. Chem. Phys.* **1993**, *98*, 7361−7374.
(41) McRae, R. P.; Schenter, G. K.; Garrett, B. C.; Svetlicic, Z.; Truhlar, D. G. Variational transition state theory evaluation of the rate constant for proton transfer in a polar solvent. *J. Chem. Phys.* **2001**, *115*, 8460−8480.
(42) Antoniou, D.; Schwartz, S. D. A molecular dynamics quantum Kramers study of proton transfer in solution. *J. Chem. Phys.* **1999**, *110*, 465−472.
(43) Antoniou, D.; Schwartz, S. D. Quantum proton transfer with spatially dependent friction: Phenol-amine in methyl chloride. *J. Chem. Phys.* **1999**, *110*, 7359−7364.
(44) Kim, S. Y.; Hammes-Schiffer, S. Molecular dynamics with quantum transitions for proton transfer: Quantum treatment of hydrogen and donor−acceptor motions. *J. Chem. Phys.* **2003**, *119*, 4389−4398.
(45) Yamamoto, T.; Miller, W. H. Path integral evaluation of the quantum instanton rate constant for proton transfer in a polar solvent. *J. Chem. Phys.* **2005**, *122*, No. 044106 (13 pages).
(46) Marcus, R. A.; Sutin, N. Electron Transfers in Chemistry and Biology. *Biochim. Biophys. Acta* **1985**, *811*, 265−322.
(47) Warshel, A. Dynamics of reactions in polar solvents. Semiclassical trajectory studies of electron-transfer and proton-transfer reactions. *J. Phys. Chem.* **1982**, *86*, 2218−2224.
(48) Carter, E.; Ciccotti, G.; Hynes, J. T.; Kapral, R. Constrained reaction coordinate dynamics for the simulation of rare events. *Chem. Phys. Lett.* **1989**, *156*, 472−477.

AR030281Q